Deep Understanding Degradation Mechanism of Green Biopolyester Nanocomposites with Various Cellulose Nanocrystal Based Nanohybrids

Gaojun Lu
Zhejiang Sci-Tech University
Jingli Zhu
HUAFON GROUP CO., LTD
Hou–Yong Yu (phdyu@zstu.edu.cn)
Zhejiang Sci-Tech University https://orcid.org/0000-0002-6543-5924
Meijin Jin
HUAFON GROUP CO.,LTD
Somia Yassin Hussain Abdalkarim
Zhejiang Sci-Tech University
Yong Wei
HUAFON GROUP CO., LTD

Research Article

Keywords: Cellulose nanocrystal, Zinc oxide, Morphologies, Composites, Degradation

Posted Date: May 7th, 2021

DOI: https://doi.org/10.21203/rs.3.rs-438980/v1

Abstract

Oceans and soils have been contaminated with traditional plastic due to their lack of degradability. Therefore, green biopolymer composites reinforced with cellulose nanocrystal-zinc oxide hybrids (ZnO hybrids) with good biodegradation ability provide a positive impact on reducing environmental challenges. In this work, the effect of various morphologies of ZnO hybrids on the biodegradation ability of poly(butylene adipate-co-terephthalate), PBAT) under seawater, soil burial, and UV aging conditions were investigated. Sheet-like ZnO hybrids (s-ZnO hybrid) could efficiently enhance mechanical, UV-blocking properties and biodegradation ability of PBAT. Compared to neat PBAT films, the best tensile strength of PBAT nanocomposite with 2 wt.% s-ZnO hybrid was increased by 15.1%, meanwhile this nanocomposite films showed the highest biodegradation rate after 80 days of soil degradation and 90 days of seawater degradation. Besides, three possible biodegradation mechanisms of green PBAT nanocomposite films were presented, hinting that such PBAT nanocomposite have great promising packaging applications.

Highlights

- PBAT nanocomposites with various morphologies of CNC-ZnO hybrids are prepared
- UV shielding and mechanical properties were improved by adding various CNC-ZnO hybrids
- Sheet-like CNC-ZnO hybrids gave the best reinforcing efficiency on PBAT than other hybrids
- Three possible biodegradation mechanisms of PBAT nanocomposites are provided

Introduction

In earlier 2021, China has announced that single-use plastic bags from non-degradable polymers would be banned across all cities. Particularly food packaging industry should minimize the use of single-use plastic items by 30%. Our oceans and soils have been contaminated with plastic due to their lack of degradability leading to serious plastic pollution (white pollution) (Geyer et al. 2017). Besides, non-degradable polymers such as polyethylene (PE), polypropylene (PP), polystyrene (PS) have widely used in food packaging materials and ultimately accumulate in the bodies could seriously cause damaging effects on human health (Mohanty et al. 2000; Kumagai et al. 2019). As a result, the development of fully biodegradable food packaging materials aimed at the replacements of non-degradable is to be prospective (Haider et al. 2019; Wang et al. 2021). Numerous biodegradables have already been used in packaging materials, among which PBAT polymer is mostly used due to biodegradability, and extreme flexibility (Mohammadi et al. 2020). However, low mechanical resistance, weak UV-blocking, and especially unclear degradation mechanism hindering their wide usages in food packaging application (Moustafa et al. 2017; Ye et al. 2020).

Recently, natural cellulose nanocrystals (CNC) with high strength and excellent biodegradability were believed as ideal reinforced agent to enhance the mechanical strength and biodegradability rate of PBAT (Lai et al. 2020), but neat CNC cannot endow the PBAT with UV-blocking performance, which will affect

its lifetime for packaging materials. Fortunately, some metal, metal oxide, or plant such as (rosin, graphene oxide (GO), chitosan, zinc oxide (ZnO) and so on) (Xing et al. 2019; Khan et al. 2020; Li et al. 2020a) were functionalized into CNC as hybrids materials into the polymer matrix to provide functional nanocomposites with excellent UV shielding and enhance biodegradability. Especially, among all the hybrids, CNC-ZnO hybrids show more excellent antimicrobial, photocatalytic activity, ultrahigh UV shielding properties, which can act as reinforcing agent to improve properties of biopolymers reported by our research groups (Abdalkarim et al. 2018; Wang et al. 2019). However, to our knowledge, no study has investigated the biodegradability behavior of PBAT nanocomposite films with different morphological of CNC-ZnO hybrids namely (ZnO hybrids) under soil burial, seawater, and UV aging conditions.

Therefore, this present study designed and fabricated various morphologies of ZnO hybrids namely (r-ZnO, d-ZnO, and s-ZnO hybrids) and then introduced into PBAT matrix through solution casting. Moreover, the effect of various ZnO hybrids on the thermal stability, UV shielding, and mechanical properties of resultant PBAT nanocomposite films were evaluated. More importantly, the biodegradation ability and mechanism of neat PBAT and PBAT nanocomposites with various ZnO hybrids under soil burial, seawater, and UV aging conditions were also studied, which provides a theoretical basis for environmentally friendly food packaging materials in the future.

Experimental Section

Materials

Commercial Microcrystalline cellulose (MCC) was purchased from Shanghai Chemical Reagents (Shanghai, China). The citric acid ($C_6H_8O_7$), sodium hydroxide (NaOH), zinc chloride ($ZnCl_2$), chloroform ($CHCl_3$), was purchased from Aladdin biochemical Polytron Technologies Inc. Hydrochloric acid (HCl) was supplied by Hangzhou Shuanglin Chemical Reagent Company. Poly (butylene adipate-co-terephthalate) (PBAT, Mn = 1.0 ×10^5) was supplied by Xinfu Pharmaceutical Co. Ltd, all materials were used as received without further purification.

Synthesis of ZnO hybrids

CNC was prepared by our previous synthesis method, using citric acid ($C_6H_8O_7$)/hydrochloric acid mixed hydrolysis of MCC. For the preparation of CNC-ZnO hybrids namely (ZnO hybrids), 0.04 g of CNC (dried powder) and 0.2726 g of $ZnCl_2$ were dissolved in 40 mL deionized water, then, under continuous stirring, the pH value of the mixture was adjusted to 7 by using NaOH solution (0.5mol/L). After that When the mixture was heated to 80°C, NaOH solution (0.1 mol/L) was added dropwise to adjust the pH to 10.3 and 10.5, respectively. Finally, transfer the mentioned solution to two 40mL screw-covered glass bottles, stored at 80°C for 24 h in an oven. Under these conditions, rice-like and rod-like ZnO hybrids were obtained, the resulting hybrids were designated as r-ZnO, and d-ZnO hybrids according to the structure of nanoparticles, respectively. For sheet-like ZnO hybrids, about (5.0 mmol) $ZnCl_2$, 10 g CNC suspension (4.5 g/L), and NaOH (15.0 mmol), were added into screw-capped glass vials, then the mixture was added to

25 mL deionized water with strong stirring at room temperature, and stored at 80°C for 24 h in an oven. Finally, the sheet-like ZnO hybrids were washed several times with deionized water and dried at 60°C for 12 hours, the resulting hybrids were designated as s-ZnO hybrids.

Fabrication of nanocomposites

The PBAT nanocomposite films with ZnO hybrids were prepared by the solution casting method. In brief, the mass ratio of PBAT to chloroform was 1:9, for a certain amount of PBAT around were completely dissolved in chloroform under 70 ℃ water bath conditions. The resultant PBAT solutions were used as the working solution for nanocomposite films. After that ZnO hybrids with different morphologies with a mass fraction of 2% (based on the weight of PBAT) were dispersed in chloroform under ultrasonic treatment for 30 min. The resultant ZnO hybrids suspension is added to the PBAT solutions, until a uniform dispersion was obtained the mixture solution was stirred under ambient conditions for 24 hours, and then coated solution evenly on the glass. The PBAT nanocomposite films with a thickness of about 30–40 μm were obtained which were named PBAT, r-ZnO, d-ZnO, s-ZnO. Characterizations of ZnO hybrids and their nanocomposites including field emission scanning electron microscopy (FE-SEM), UV − vis spectrophotometer, Fourier transforms infrared spectroscopy (FTIR), Thermal gravimetric analysis (TGA), and Tensile tests are provided in Supporting Information.

Characterization

Soil burial degradation was carried out at the soil about 10 cm deep from the ground under the cypress trees of Zhejiang Sci-Tech University according to our previously reported methods (Wang et al. 2019). The PBAT nanocomposite films with an area of 32 cm^2 were dried in an oven at 60°C for 24 h before degradation. Regularly, the samples were taken out, washed by deionization water, and weighed again after being dried at 60°C for 24 h. The weight loss of PBAT nanocomposite films in soil was calculated using the following:

$$Weight\ loss\ (\%) = \frac{m_a - m_b}{m_a} \qquad (1)$$

where m_a is the mass of samples before soil degradation, m_b is the mass of samples after degradation. Seawater degradation behavior: the samples (3×3 cm^2) of PBAT nanocomposite films were sealed in a glass tube with 30 mL of homemade seawater which was made by deionized water and sea salt extracted from natural seawater. The height of the seawater was recorded with a scale, specific environment in homemade seawater was based on the indoor temperature and lighting environment. Due to the continuous evaporation of the water body during the experiment, the method of supplementing distilled water was used to maintain the height of the water surface. To maintain the salinity of the water body, the homemade seawater was changed every half a month. Similarly, the samples were washed and dried at regular intervals to evaluate the effect of seawater degradation of PBAT nanocomposites. The weight loss of PBAT nanocomposite films in seawater was calculated using the above eq.

The ultraviolet aging of PBAT nanocomposite films was conducted in a UV irradiation oven. The samples (3×3 cm^2) were exposed to UV lamps that the temperature was adjusted at 60°C. All samples are exposed on the same side of the UV lamp. To analyze the process of UV aging, the PBAT nanocomposite films were UV aged for 8, 16 weeks, separately.

Results And Discussion

Morphology observation

The morphologies structure of CNC and ZnO hybrids were shown in (Fig. 1a-d). In Fig. 1a, the shape of neat CNC is a nanorod with a diameter of 11.3 mm and a length of 187.2 ± 21 nm. The monomer zinc hydroxide Zn $(OH)_2$ was formed by the combination of anion OH^- and cation Zn^{2+}, and Zn $(OH)_2$ dehydrates to form elementary particles of zinc oxide (ZnO). Under this system, the COO^- from carboxyl groups on the CNC template repelled each other with OH^- and competed to attract the cationic Zn^{2+}, different morphologies of ZnO hybrids were obtained which was due to the different ratio and concentration of the OH^- and the carboxylate anion (COO^-) from carboxyl groups on the CNC template (Guan et al. 2019). When the OH^- concentration was low (pH = 10.3), the r-ZnO hybrids was uniformed with the diameter of 90–500 nm, the length of 230–1500 nm (Fig. 1b). With the increasing of OH^-concentration, the d-ZnO hybrids with average diameter of 80 ± 20nm, average length of 220 ± 30 nm was obtained (Fig. 1c). And as shown in Fig. 1d, the s-ZnO hybrids with average length of 290–830 nm, the average diameter of 206 ± 15 nm, and the sheet thickness of 40–68 nm were found.

The cross-section morphologies of neat PBAT and PBAT nanocomposite films are shown in (Fig. 1e-h). As we know, the dispersion of hybrids in the polymer has a great influence on improving its performance (Xu et al. 2016). As shown in Fig. 1e, neat PBAT film showed a smooth fracture surface without any fillers. All nanocomposite films had a relatively smooth cross-section, which indicated that ZnO hybrids had good dispersibility within the PBAT matrix. It was clear that the s-ZnO hybrids were dispersed more homogeneously in the PBAT matrix, compared with other nanocomposites, which was attributed to the strong intermolecular interaction between the PBAT matrix and the s-ZnO hybrids with the larger specific surface area.

Chemical structure and thermal properties

The FTIR spectra of neat PBAT and PBAT nanocomposite films are shown in (Fig. 2a, b). The neat PBAT spectrum displayed characteristic bands at 1452, 1409, 1386, and 1358 cm^{-1}, attributing to the phenylene stretching group (Cai et al. 2013). Also, the absorption peak at 2950 cm^{-1} was assigned to C-H asymmetric stretching modes of CH_2 groups and aromatic ones. The peak of the ester carbonyl (C = O) stretching vibration was located at 1719 cm^{-1} (Han et al. 2020). Besides, the peaks appearing between 1269 and 1101 cm^{-1} were assigned to the asymmetric and symmetric stretching of the C-O group, and the peak at 728 cm^{-1} correspond to the four consecutive methylene groups of PBAT matrix (Mohanty

and Nayak 2012; Tavares et al. 2018). Compared to neat PBAT, a new peak at 452 cm^{-1} of PBAT nanocomposite films was obtained that was ascribed to ZnO stretching vibration, which demonstrated that ZnO hybrids were effectively introduced to the PBAT matrix (Arputharaj et al. 2017).

Peak deconvolution for the PBAT nanocomposite films with ZnO hybrids was shown in (Fig. 2b, and Fig. S1), and the $F_{H\text{-}CO}$ value was obtained through curve-fitting of Gauss-Lorentz spectral function (Fig. 2a) (Yu et al. 2017). PBAT nanocomposite films showed the highest $F_{H\text{-}CO}$ by adding s-ZnO hybrids, indicated that more hydrogen bonds were formed between the hydroxyl group of the s-ZnO hybrids and the carbonyl group of the PBAT matrix, which was mainly due to the better dispersion of s-ZnO hybrids in the PBAT matrix.

The thermal stability of neat PBAT and its nanocomposite films were evaluated through TGA and DTG. As shown in (Fig. 2c, d), neat PBAT gave a single thermal degradation peak between 330°C and 530°C, while PBAT nanocomposite films had a two-step degradation process with two lower DTG peaks. The first degradation process with initial degradation temperature (T_0) of approximately 259.9°C and maximum degradation temperature (T_{max}) of about 380.2°C was attributed to thermal degradation of cellulose as reported that the degradation temperature of cellulose at 200–360°C (Sai and Mitra 2020). The temperature of PBAT nanocomposite films was lower than that of neat PBAT, owing to the high thermal conductivity and catalytic properties of ZnO hybrids (Lizundia et al. 2016).

Mechanical property

It was well known that the dispersion state of the filler, the crystallinity of the matrix, and the interaction between the filler and the matrix affect the mechanical properties of the biopolymer composites (Diez-Pascual and Diez-Vicente 2014; Venkatesan and Rajeswari 2017). The mechanical properties of PBAT nanocomposite films were evaluated by tensile tests, and the typical stress-strain curves are shown in Fig. 2e. The tensile strength of neat PBAT was about 11.60 MPa, and the tensile strength increased with the addition of ZnO hybrids, which indicated that the mechanical properties of PBAT nanocomposite films were improved by incorporating rigid ZnO hybrids at lower concentrations. Compared with other nanocomposites, PBAT nanocomposite films with s-ZnO hybrids showed the highest tensile strength up to (13.35 MPa), the tensile strength increased by 15.1%, which could be due to the uniform dispersion of s-ZnO hybrids in the PBAT matrix, stronger interfacial adhesion, and increased crystallinity, which were supported by SEM, FTIR and DSC results (Fig. 1h, Fig. 2b, and Fig. S2).

On the other hand, ZnO hybrids with different morphologies induced obvious changes on the toughness of the PBAT matrix. The strain at break was improved by adding d-ZnO hybrids. However, the strain of the PBAT nanocomposite films with r-ZnO hybrids was significantly reduced by 4%, due to its inhomogeneous dispersion and partial agglomeration in the PBAT matrix, which limited the ductile flow of the polymer chains. This phenomenon indicated that the dispersion of hybrids had a greater effect on the flexibility of nanocomposites.

Optical performance

The optical properties of the PBAT nanocomposite films in the range of 200–800 nm were shown in Fig. 3 The neat PBAT film had the highest transparency with the transmittance of 75% at 800 nm, while the transmittance for PBAT nanocomposite films was still as high as 73% at the wavelength of 800 nm that indicated the ZnO hybrids had a good dispersion in the PBAT matrix. As for UV barrier properties, neat PBAT had a poor performance in the UVA range (320-400nm) but absorbed almost UVB light (280–320 nm) of 94% and all the range below due to the carbonyl functions and conjugated double bonds of PBAT matrix (Masson et al. 2004).

The addition of ZnO hybrids improved the UV barrier properties of the UVA region (320-400nm) as shown in Table 1. The PBAT nanocomposite films with s-ZnO and d- -ZnO hybrids absorbed 69.1%, 59.3% of UVA light, respectively, which was due to the ZnO has unique electro-optical properties and efficient UV absorption capabilities with a wide bandgap (corresponding to 376 nm), that the matches or exceeds its bandgap energy can be absorbed (John et al. 2011). It can be seen from Table 1 the UPF value of neat PBAT was about 6.24, and the nanocomposite films had the highest UPF value (12.36) after adding the s-ZnO hybrids, while the UPF value of PBAT nanocomposite films with r-ZnO hybrids was only improved by 32%, which was attributed to the agglomerates of r-ZnO hybrids in PBAT matrix (Rajagopalan and Khanna 2013).

Table 1
Percentage of Blocking from UVA and UVB radiation and UPF values of neat PBAT and PBAT nanocomposite films with various morphologies ZnO hybrids

Samples	Percentage blocking		UPF value
	UVA	UVB	
PBAT	48.02%	94.02%	6.24
Rice-like	59.28%	95.63%	8.29
Rod-like	66.17%	95.81%	9.58
Sheet-like	72.25%	96.70%	12.36

Soil burial and seawater degradation behavior

To study the degradation of PBAT nanocomposite films in soil, the PBAT nanocomposite films were characterized by weight loss, SEM, and FTIR before and after degradation. The weight loss of neat PBAT and PBAT nanocomposite films after degradation in the soil can be seen in Fig. 4a. The result showed that the weight loss of all PBAT films increased with time, which indicated that all the films had been degraded. However, after 80 days of degradation in the soil, the weight loss of neat PBAT was only about 2%, which was the lowest of all samples, similar results have been reported in the literature (Pinheiro et al. 2017). And it can be observed that the PBAT nanocomposite film with s-ZnO hybrids showed a faster degradation rate, owing to the higher specific surface area of s-ZnO which were helpful to contact with water to accelerate the degradation.

The weight loss of neat PBAT and PBAT nanocomposite films after degradation in seawater was shown in Fig. 4b. Neat PBAT showed minimal degradation after 90 days only about 1.2%. The PBAT nanocomposite film was degraded by about 5.23% after 90 days by adding s-ZnO hybrids. Compared with the soil degradation, the degradation of PBAT films in seawater was slower, mainly due to the characteristics of the marine environment (high salinity, dilute nutrients, and fewer bacterial colonies). Therefore, hydrolytic degradation was the main method for PBAT degradation in seawater.

The SEM micrographs of neat PBAT and PBAT nanocomposite films showed changes in morphology and appearance after 80 days of degradation (Fig. 6a). It can be found that after 80 days of degradation, the surface of all PBAT films became very rough, which indicated that the PBAT nanocomposite film has been degraded. Impressively, compared to neat PBAT, many corrosive holes with some cracks were observed of the PBAT nanocomposite films, some factors can explain this: on the one hand, the hydrophilic property of ZnO hybrids can make water accumulate and promote hydrolysis (Fig. 6b). On the other hand, CNC provided nutrients for microorganisms in the soil and promotes the decomposition of the nanocomposite films by microorganisms (Someya et al. 2007; Pinheiro et al. 2017). And that the Zn^{2+} would be generated when ZnO encountered acidic substances in the soil, thereby more pores were formed in the PBAT matrix which accelerated the biodegradation rate of the PBAT nanocomposite films (Fig. 5).

After 90 days of degradation in seawater, the SEM micrograph of the neat PBAT and PBAT nanocomposite films was shown in Fig. 6c. The surface of all PBAT films became rough, especially a lot of grooves on the surface of the PBAT nanocomposite films were observed. However, there were almost no cracks in the neat PBAT film that could be observed, which could be attributed to the fact that the seawater cannot easily penetrate the highly ordered crystalline regions of PBAT and the hydrolytic degradation mainly dependent on the structure of the amorphous region (Laycock et al. 2017; Venkatesan et al. 2018). The expansion and the stress of PBAT nanocomposite films would be generated by the absorption of water on the amorphous crystal interface, which led to the generation of microbubbles and further degradation. In particular, the surface of the nanocomposite films was severely corroded with many pores scattered on the surface, perhaps this was due to the simple fact that ZnO hybrids provided the sites for seawater to enter the PBAT nanocomposite films (Li et al. 2020b)and that the ZnO hybrids were immersed in seawater and caused swelling to provide the larger surface area to promote hydrolytic degradation (Fig. 5).

To further understand the degradation mechanism of PBAT nanocomposite films in soil and seawater, the chemical structure changes before and after degradation of PBAT nanocomposite films were analyzed by FTIR (Fig. 4c, d), represented by neat PBAT and nanocomposite membranes added with s-ZnO. Since hydrolysis was one of the initial processes of biodegradation, the ester bond was randomly broken along with the hydrolysis. Therefore, whether it was soil degradation or seawater degradation, it was initially through hydrolysis. And it can be analyzed by hydroxyl (O-H) and carbonyl (C = O) groups to study the mechanism of PBAT degradation. As shown in (Fig. 4c, d), the hydroxyl peak of neat PBAT and PBAT nanocomposite films were enhanced after soil degradation or seawater degradation, while the C = O ($1740cm^{-1}$) peak weakens. However, compared to seawater degradation, it can be observed that the

chemical structure of all PBAT films after soil degradation changed more obviously (Fig. 4c), which was mainly attribute to that, in soil degradation, the ester bond of PBAT was more easily destroyed by the action of water, oxygen, and microorganisms. Eventually, PBAT films were degraded and completely decomposed into carbon dioxide and water (Venkatesan et al. 2018; Zumstein et al. 2018).

Ultraviolet aging behavior

According to literature reports, PBAT with two different types of photosensitive groups (benzene ring, and carbonyl group) led to the chain scission through the Norrish I or Norrish Ⅱ reaction during UV aging. Besides, after the formation of free radicals through Norris I reaction, there was a photooxidation process (Al-Itry et al. 2012). That can be proved by the changes of characteristic peaks (C-O, C = O) of PBAT in the FTIR spectrum (Fig. 7a) (Zhu et al. 2019). The positions of pure PBAT and PBAT nanocomposite films have not changed significantly after UV aging, while the peak intensity was changed. After 16 weeks of UV aging, the absorption peak intensity of C = O at 1719 cm^{-1} and C-O at 1269 cm^{-1} were both decreased, which indicated that after UV aging, part of C-O bonds in the PBAT molecular chain were broken to form free radicals, while cracking and oxidation occurred in the part C-O bonds of PBAT matrix under UV light irradiation, and after that free radicals was formed and CO_2 was released (Fig. 7b) (Kijchavengkul et al. 2011). Among them, the absorption peak intensity of PBAT with s-ZnO hybrids changed more obviously, which is mainly due to ZnO catalyzed the photodegradation.

That can also be further proved by the SEM (Fig. 7c-e). With the increase of the UV light irradiation time, the surface of the pure PBAT and PBAT nanocomposite film became rough. At the same time, many cracks can be observed on the surface of the films after 16 weeks of UV aging, which can be attributed to the cleavage of the PBAT chain and the cross-linking reaction during the UV aging process. In particular, more holes of PBAT nanocomposite films with s-ZnO can be observed after 16 weeks of UV aging, which was consistent with the FTIR results (Fig. 7a), proved that the fastest photodegradation rate was obtained for PBAT nanocomposite films with s-ZnO hybrids.

Conclusion

In this study, neat PBAT and PBAT nanocomposite films were successfully prepared in order to study the effect of different morphology of ZnO hybrids on the mechanical, UV-blocking properties and biodegradability of PBAT nanocomposite film. The s-ZnO hybrids had the most obvious impact on the performance of the PBAT nanocomposite films, in which the values of UPF were increased up to 12.4 and the tensile strength was increased by 15.1%. In particular, degradation ability of PBAT nanocomposite films with ZnO hybrids has been significantly improved, mainly due to the hydrophilicity of CNC to accelerate the hydrolysis of ester bonds and CNC and thus provide the nutrients for microorganisms. This work presents the possible biodegradation mechanisms for green packaging materials of PBAT nanocomposite films under seawater, soil burial, and UV aging conditions.

Declarations

Funding The authors declare no competing financial interest.

Conflict of interest All authors declare that they have no conflict of interest.

Human and animal rights This manuscript does not contain any studies with human participants or animals performed by any of the authors.

Author's contributions Gaojun Lu: Conceptualization, Data curation, Investigation, Writing-original draft, Writing-review & editing. Jingli Zhu: Project administration, Writing-review & Software. Houyong Yu: Methodology, Writing-review & editing, Supervision. Meijin Jin: Investigation, Project administration. Somia Yassin Hussain Abdalkarim: Conceptualization, Writing - review & editing. Yong Wei: Investigation, Supervision.

Acknowledgements The work was supported by Zhejiang Provincial Natural Science key Foundation of China (LZ20E030003), the Fundamental Research Funds of Zhejiang Sci-Tech University (2019Q001) and the Young Elite Scientists Sponsorship Program by CAST (2018QNRC001).

References

1. Abdalkarim SYH, Yu H-Y, Wang C et al (2018) Sheet-like Cellulose Nanocrystal-ZnO Nanohybrids as Multifunctional Reinforcing Agents in Biopolyester Composite Nanofibers with Ultrahigh UV-Shielding and Antibacterial Performances. ACS Appl Bio Mater 1:714–727. https://doi.org/10.1021/acsabm.8b00188
2. Al-Itry R, Lamnawar K, Maazouz A (2012) Improvement of thermal stability, rheological and mechanical properties of PLA, PBAT and their blends by reactive extrusion with functionalized epoxy. Polym Degrad Stab 97:1898–1914. https://doi.org/10.1016/j.polymdegradstab.2012.06.028
3. Arputharaj A, Nadanathangam V, Shukla SR (2017) A simple and efficient protocol to develop durable multifunctional property to cellulosic materials using in situ generated nano-ZnO. Cellulose 24:3399–3410. https://doi.org/10.1007/s10570-017-1335-5
4. Cai Y, Lv J, Feng J (2013) Spectral Characterization of Four Kinds of Biodegradable Plastics: Poly (Lactic Acid), Poly (Butylenes Adipate-Co-Terephthalate), Poly (Hydroxybutyrate-Co-Hydroxyvalerate) and Poly (Butylenes Succinate) with FTIR and Raman Spectroscopy. J Polym Environ 21:108–114. https://doi.org/10.1007/s10924-012-0534-2
5. Diez-Pascual AM, Diez-Vicente AL (2014) ZnO-reinforced poly(3-hydroxybutyrate-co-3-hydroxyvalerate) bionanocomposites with antimicrobial function for food packaging. ACS Appl Mater Interfaces 6:9822–9834. https://doi.org/10.1021/am502261e
6. Geyer R, Jambeck JR, Law KL (2017) Production, use, and fate of all plastics ever made. Sci Adv 3:. https://doi.org/10.1126/sciadv.1700782
7. Guan Y, Yu HY, Abdalkarim SYH et al (2019) Green one-step synthesis of ZnO/cellulose nanocrystal hybrids with modulated morphologies and superfast absorption of cationic dyes. Int J Biol

Macromol 132:51–62. https://doi.org/10.1016/j.ijbiomac.2019.03.104

8. Haider TP, Völker C, Kramm J et al (2019) Plastics of the Future? The Impact of Biodegradable Polymers on the Environment and on Society. Angew Chemie Int Ed 58:50–62. https://doi.org/https://doi.org/10.1002/anie.201805766
9. Han Y, Shi J, Mao L et al (2020) Improvement of Compatibility and Mechanical Performances of PLA/PBAT Composites with Epoxidized Soybean Oil as Compatibilizer. Ind Eng Chem Res 59:21779–21790. https://doi.org/10.1021/acs.iecr.0c04285
10. John A, Ko HU, Kim DG, Kim J (2011) Preparation of cellulose-ZnO hybrid films by a wet chemical method and their characterization. Cellulose 18:675–680. https://doi.org/10.1007/s10570-011-9523-1
11. Khan MZ, Militky J, Baheti V et al (2020) Growth of ZnO nanorods on cotton fabrics via microwave hydrothermal method: effect of size and shape of nanorods on superhydrophobic and UV-blocking properties. Cellulose 27:10519–10539. https://doi.org/10.1007/s10570-020-03495-x
12. Kijchavengkul T, Auras R, Rubino M et al (2011) Formulation selection of aliphatic- aromatic biodegradable polyester film exposed to UV/solar radiation. Polym Degrad Stab 96:1919–1926. https://doi.org/10.1016/j.polymdegradstab.2011.07.001
13. Kumagai S, Yamamoto M, Takahashi Y et al (2019) Impact of Common Plastics on Cellulose Pyrolysis. Energy Fuels 33:6837–6841. https://doi.org/10.1021/acs.energyfuels.9b01376
14. Lai L, Wang S, Li J et al (2020) Stiffening, strengthening, and toughening of biodegradable poly(butylene adipate-co-terephthalate) with a low nanoinclusion usage. Carbohydr Polym 247:116687. https://doi.org/10.1016/j.carbpol.2020.116687
15. Laycock B, Nikolić M, Colwell JM et al (2017) Lifetime prediction of biodegradable polymers. Prog Polym Sci 71:144–189. https://doi.org/10.1016/j.progpolymsci.2017.02.004
16. Li F, Abdalkarim SYH, Yu H-Y et al (2020a) Bifunctional Reinforcement of Green Biopolymer Packaging Nanocomposites with Natural Cellulose Nanocrystal–Rosin Hybrids. ACS Appl Bio Mater 3:1944–1954. https://doi.org/10.1021/acsabm.9b01100
17. Li H, Zhang L, Lu H et al (2020b) Macro-/nanoporous Al-doped ZnO/cellulose composites based on tunable cellulose fiber sizes for enhancing photocatalytic properties. Carbohydr Polym 250:116873. https://doi.org/10.1016/j.carbpol.2020.116873
18. Lizundia E, Ruiz-Rubio L, Vilas JL, León LM (2016) Towards the development of eco-friendly disposable polymers: ZnO-initiated thermal and hydrolytic degradation in poly(l-lactide)/ZnO nanocomposites. RSC Adv 6:15660–15669. https://doi.org/10.1039/c5ra24604k
19. Masson F, Decker C, Andre S, Andrieu X (2004) UV-curable formulations for UV-transparent optical fiber coatings. Prog Org Coatings 49:1–12. https://doi.org/10.1016/s0300-9440(03)00122-x
20. Mohammadi M, Bruel C, Heuzey MC, Carreau PJ (2020) CNC dispersion in PLA and PBAT using two solvents: morphological and rheological properties. Cellulose 27:9877–9892. https://doi.org/10.1007/s10570-020-03460-8

21. Mohanty AK, Misra M, Hinrichsen G (2000) Biofibres, biodegradable polymers and biocomposites: An overview. Macromol Mater Eng 276–277:1–24. https://doi.org/10.1002/(SICI)1439-2054(20000301)276:1<1::AID-MAME1>3.0.CO;2-W
22. Mohanty S, Nayak SK (2012) Biodegradable Nanocomposites of Poly(butylene adipate-co-terephthalate) (PBAT) and Organically Modified Layered Silicates. J Polym Environ 20:195–207. https://doi.org/10.1007/s10924-011-0408-z
23. Moustafa H, Guizani C, Dupont C et al (2017) Utilization of torrefied coffee grounds as reinforcing agent to produce high-quality biodegradable PBAT composites for food packaging applications. ACS Sustain Chem Eng 5:1906–1916. https://doi.org/10.1021/acssuschemeng.6b02633
24. Pinheiro IF, Ferreira FV, Souza DHS et al (2017) Mechanical, rheological and degradation properties of PBAT nanocomposites reinforced by functionalized cellulose nanocrystals. Eur Polym J 97:356–365. https://doi.org/10.1016/j.eurpolymj.2017.10.026
25. Rajagopalan N, Khanna A (2013) Effect of size and morphology on UV-blocking property of nanoZnO in epoxy coating. Int J Sci Res Publ 3:1–14
26. Sai Prasanna N, Mitra J (2020) Isolation and characterization of cellulose nanocrystals from Cucumis sativus peels. Carbohydr Polym 247:116706. https://doi.org/10.1016/j.carbpol.2020.116706
27. Someya Y, Kondo N, Shibata M (2007) Biodegradation of poly (butylene adipate-co-butylene terephthalate)/layered-silicate nanocomposites. J Appl Polym Sci 106:730–736. https://doi.org/10.1002/app.24174
28. Tavares LB, Ito NM, Salvadori MC et al (2018) PBAT/kraft lignin blend in flexible laminated food packaging: Peeling resistance and thermal degradability. Polym Test 67:169–176. https://doi.org/10.1016/j.polymertesting.2018.03.004
29. Venkatesan R, Rajeswari N (2017) ZnO/PBAT nanocomposite films: Investigation on the mechanical and biological activity for food packaging. Polym Adv Technol 28:20–27. https://doi.org/10.1002/pat.3847
30. Venkatesan R, Rajeswari N, Tamilselvi A (2018) Antimicrobial, mechanical, barrier, and thermal properties of bio-based poly (butylene adipate-co-terephthalate) (PBAT)/Ag2O nanocomposite films for packaging application. Polym Adv Technol 29:61–68. https://doi.org/10.1002/pat.4089
31. Wang J, Wang L, Gardner DJ et al (2021) Towards a cellulose-based society: opportunities and challenges. Springer Netherlands. Cellulose 1–33
32. Wang YY, Yu HY, Yang L et al (2019) Enhancing long-term biodegradability and UV-shielding performances of transparent polylactic acid nanocomposite films by adding cellulose nanocrystal-zinc oxide hybrids. Int J Biol Macromol 141:893–905. https://doi.org/10.1016/j.ijbiomac.2019.09.062
33. Xing Q, Buono P, Ruch D et al (2019) Biodegradable UV-Blocking Films through Core–Shell Lignin–Melanin Nanoparticles in Poly(butylene adipate-co-terephthalate). ACS Sustain Chem Eng 7:4147–4157. https://doi.org/10.1021/acssuschemeng.8b05755

34. Xu H, Feng Z-X, Xie L, Hakkarainen M (2016) Graphene Oxide-Driven Design of Strong and Flexible Biopolymer Barrier Films: From Smart Crystallization Control to Affordable Engineering. ACS Sustain Chem Eng 4:334–349. https://doi.org/10.1021/acssuschemeng.5b01273
35. Ye S, Xiang X, Wang S et al (2020) Nonisocyanate CO2-Based Poly(ester- co-urethane)s with Tunable Performances: A Potential Alternative to Improve the Biodegradability of PBAT. ACS Sustain Chem Eng 8:1923–1932. https://doi.org/10.1021/acssuschemeng.9b06294
36. Yu HY, Zhang H, Song ML et al (2017) From Cellulose Nanospheres, Nanorods to Nanofibers: Various Aspect Ratio Induced Nucleation/Reinforcing Effects on Polylactic Acid for Robust-Barrier Food Packaging. ACS Appl Mater Interfaces 9:43920–43938. https://doi.org/10.1021/acsami.7b09102
37. Zhu S, Chen Y, Tang Y et al (2019) A novel nanosilica-supported ultraviolet absorber for the preparation of robust biodegradable plastic film with high ultraviolet aging resistance. Polym Compos 40:4154–4161. https://doi.org/10.1002/pc.25276
38. Zumstein MT, Schintlmeister A, Nelson TF et al (2018) Biodegradation of synthetic polymers in soils: Tracking carbon into CO2 and microbial biomass. Sci Adv 4:eaas9024. https://doi.org/10.1126/sciadv.aas9024

Figures

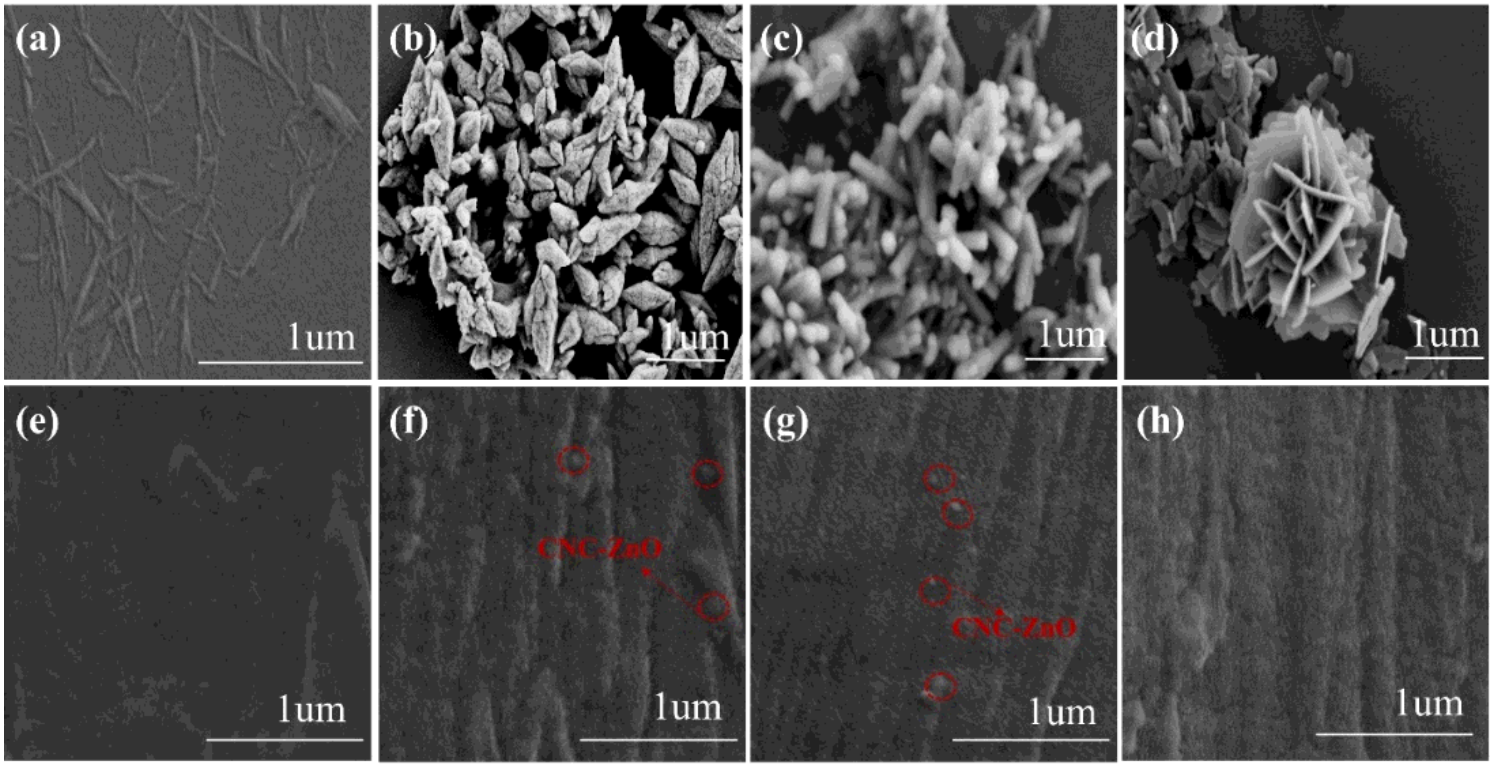

Figure 1

SEM micrographs of (a) CNCs and ZnO hybrids: (b) r-ZnO hybrids (c) d- ZnO (d) s-ZnO, and cross-sections of nanocomposites: (e) PBAT (f) r-ZnO (e) d-ZnO (h) s-ZnO.

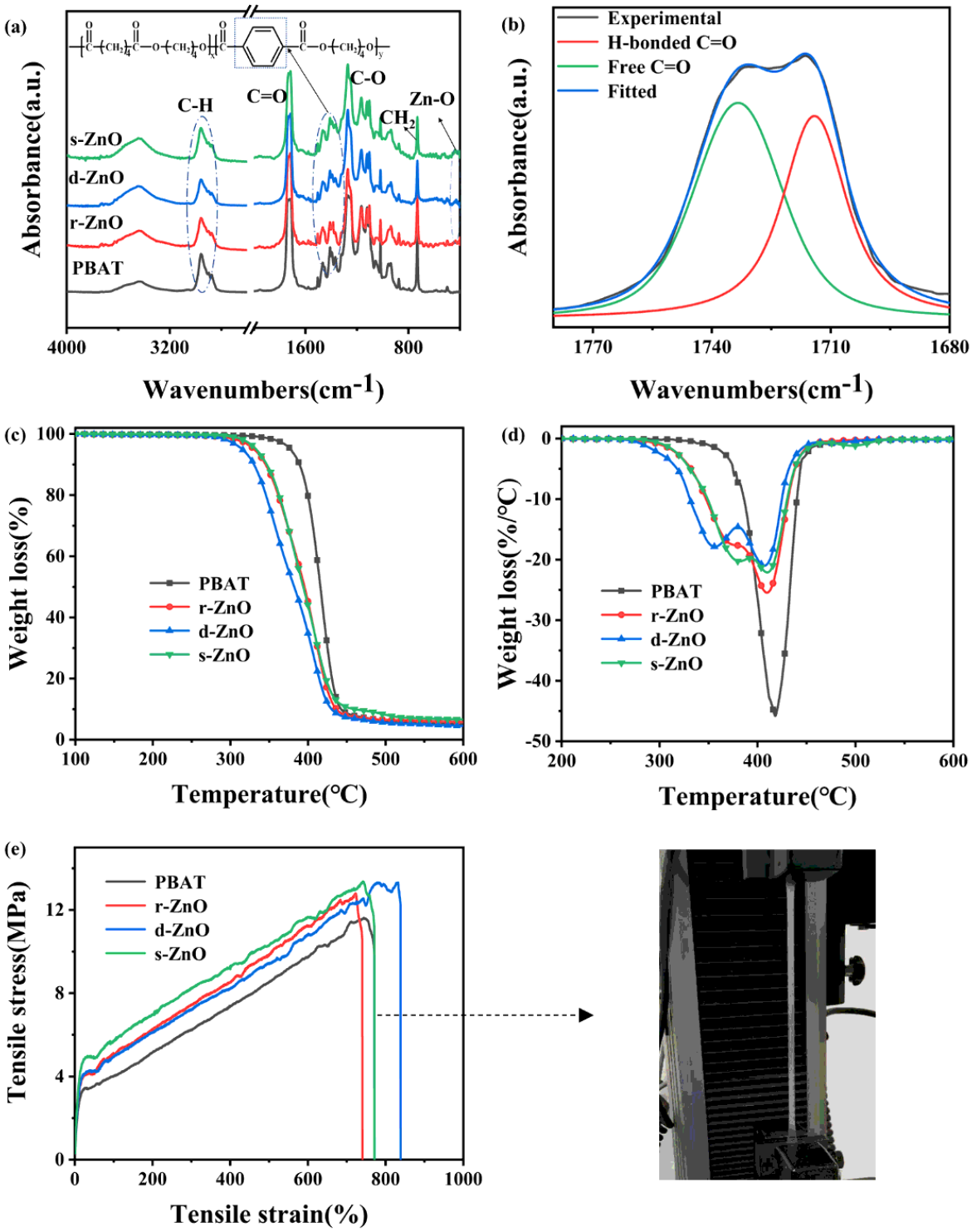

Figure 2

2 (a) FTIR spectra, (b) Peak deconvolution for the nanocomposites with s-ZnO, (c) TGA, (d) DTG curves, (e) Tensile strength of neat PBAT and PBAT nanocomposite films (the inset photographs of tensile test for neat PBAT shown in the direction).

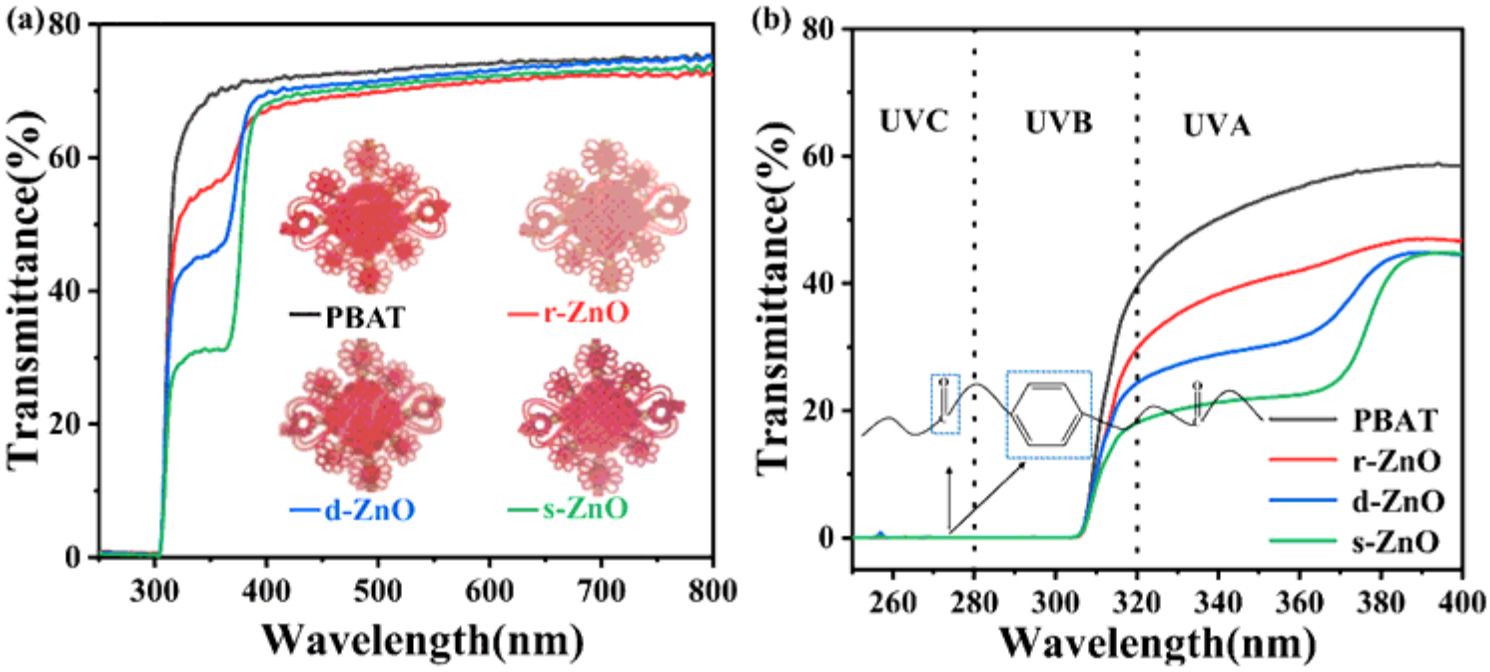

Figure 3

(a) Variation of transmittance (b) UV–vis diffuse reflectance spectra of neat PBAT and PBAT nanocomposite films with ZnO hybrids.

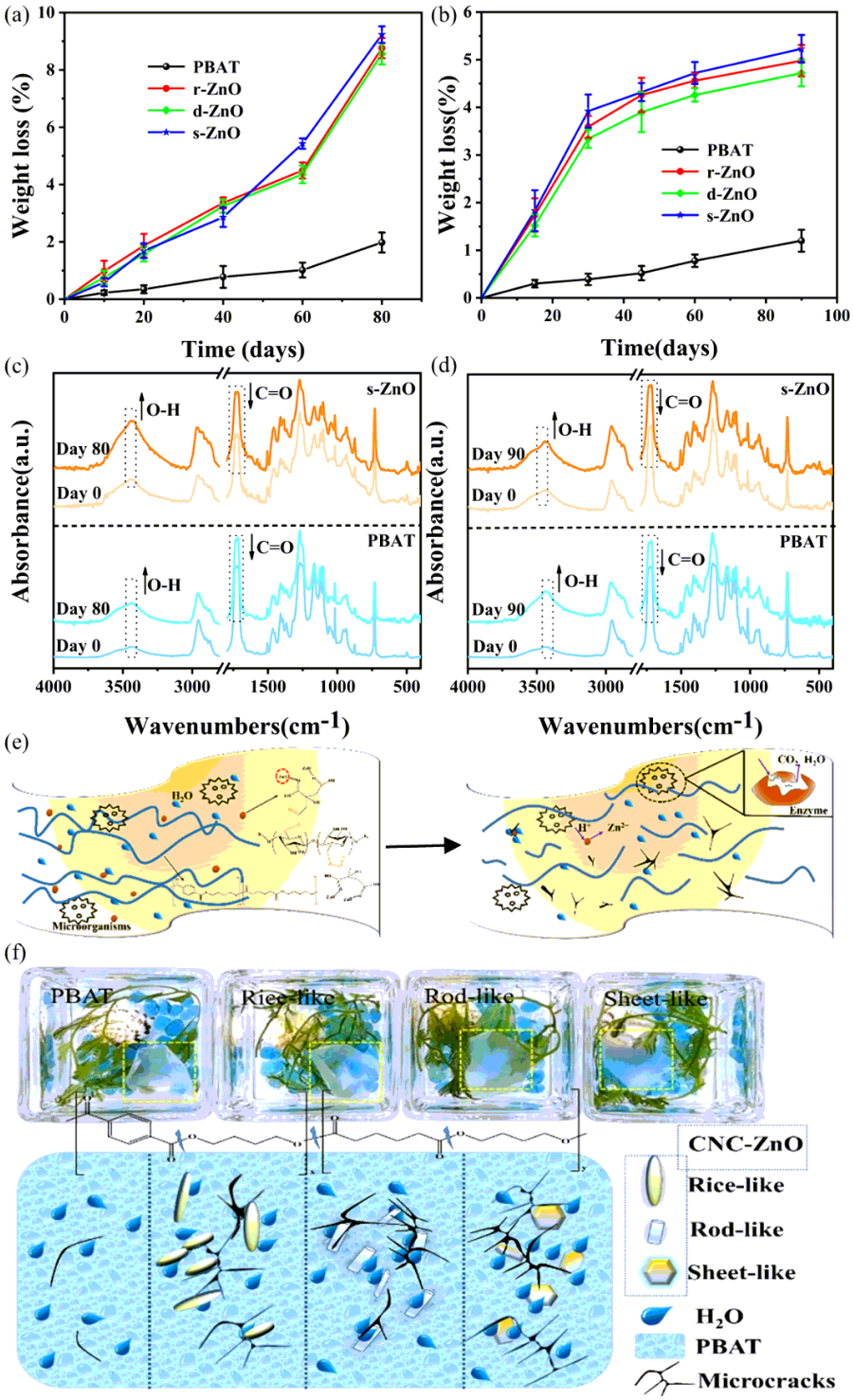

Figure 4

Weight loss of PBAT nanocomposite films after being degraded (a) in soil (b) in seawater, FTIR absorbance spectra of neat PBAT and PBAT nanocomposite film with s-ZnO before and after degradation (c) in soil (d) in seawater.

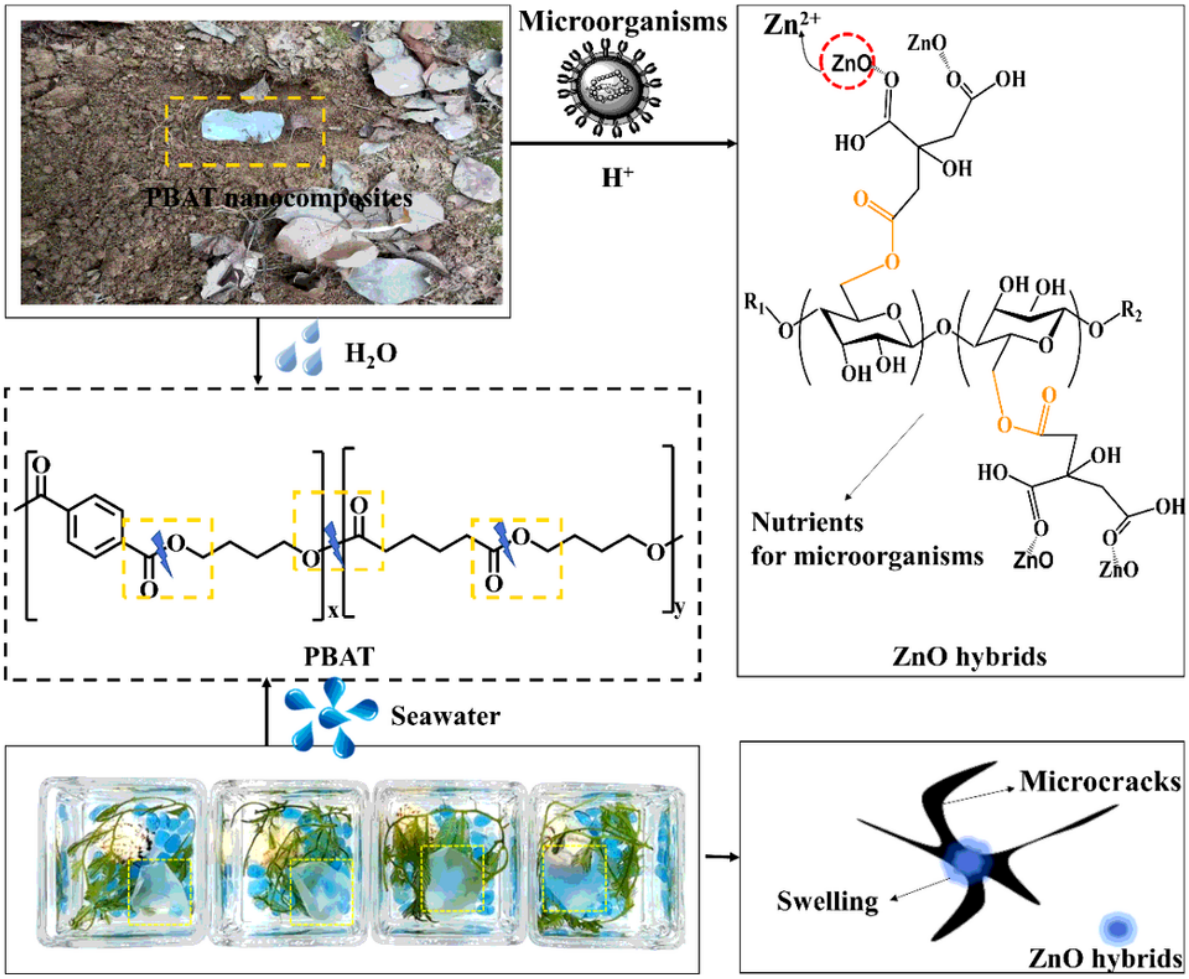

Figure 5

The schematic diagram of degradation process in soil and in seawater.

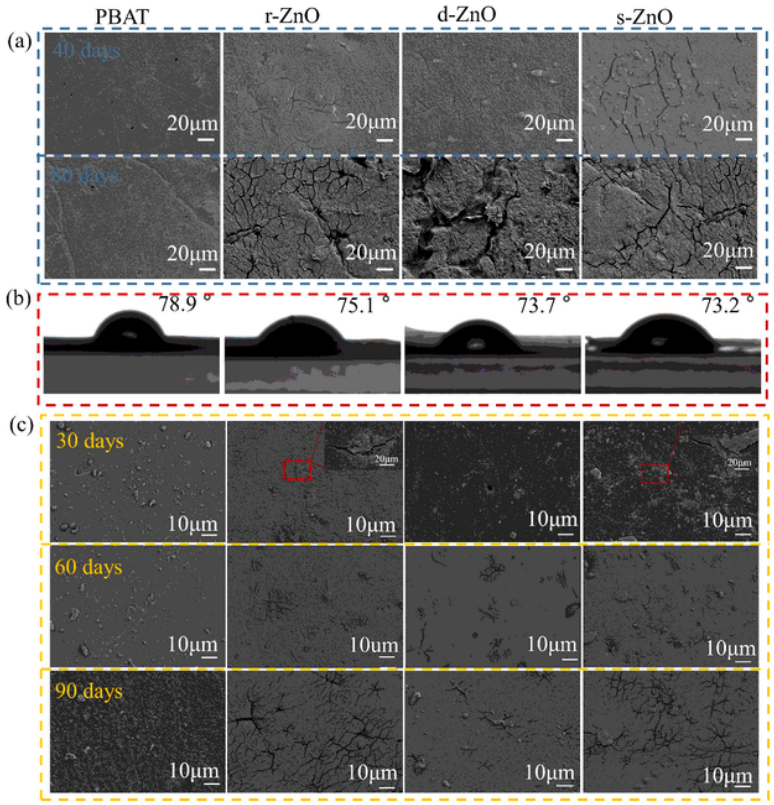

10

Figure 6

FE-SEM micrographs of neat PBAT, and PBAT nanocomposite films with different morphologies ZnO hybrids (a) after degradation in soil, (b) their contact angle, (c) after degradation in seawater

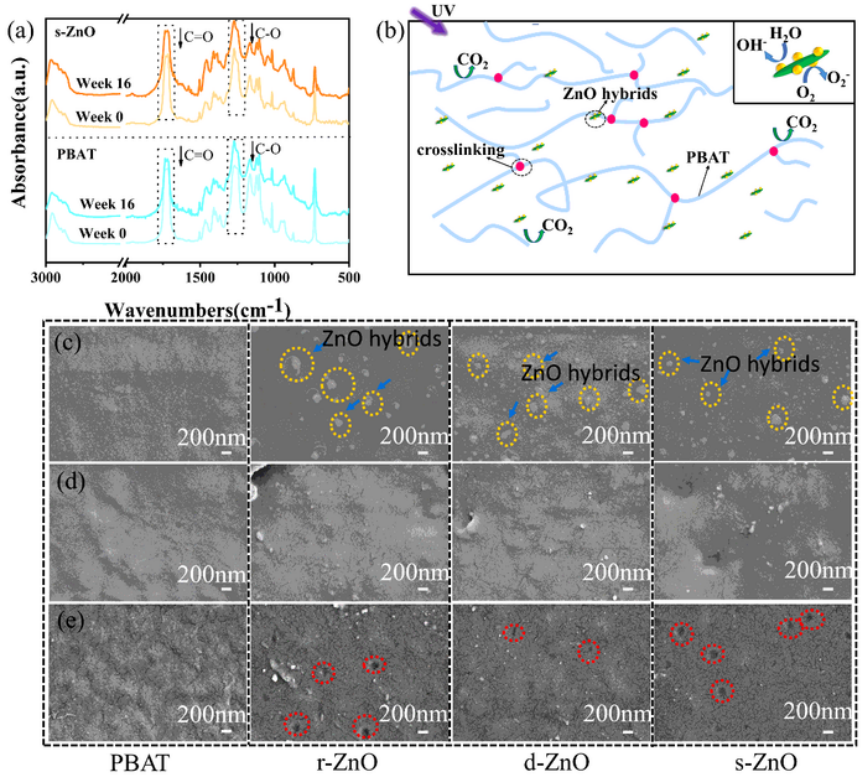

6

Figure 7

(a) FTIR spectra of neat PBAT and the PBAT nanocomposite films with s-ZnO hybrids before and after UV aging for 16 weeks (b) the schematic diagram of UV aging, FE-SEM micrographs of neat PBAT, and the PBAT nanocomposite films after being degraded for (c) 4 weeks (d) 8 weeks, and (e) 16weeks of UV aging.

Supplementary Files

This is a list of supplementary files associated with this preprint. Click to download.

- GraphicalAbstract.docx
- SuppelmenteryInformation.docx